Quantum magnetism in ultracold alkali and alkaline-earth fermion systems with symplectic symmetry

Hsiang-Hsuan Hung,[1] Yupeng Wang,[2] and Congjun Wu[1]
[1]*Department of Physics, University of California, San Diego, California 92093, USA*
[2]*Beijing National Laboratory for Condensed Matter Physics, Institute of Physics, Chinese Academy of Sciences, Beijing 100080, Peoples Republic of China*
(Received 9 March 2011; published 2 August 2011)

We numerically study the quantum magnetism of ultracold alkali and alkaline-earth fermion systems with large hyperfine spin $F = \frac{3}{2}$, which are characterized by a generic $Sp(N)$ symmetry with $N = 4$. The methods of exact diagonalization (ED) and density matrix renormalization group are employed for the large size one-dimensional (1D) systems, and the ED method is applied to a two-dimensional (2D) square lattice on small sizes. We focus on the magnetic exchange models in the Mott-insulating state at quarter-filling. Both 1D and 2D systems exhibit rich phase diagrams depending on the ratio between the spin exchanges J_0 and J_2 in the bond spin singlet and quintet channels, respectively. In one dimension, the ground states exhibit a long-range-ordered dimerization with a finite spin gap at $J_0/J_2 > 1$ and a gapless spin-liquid state at $J_0/J_2 \leqslant 1$, respectively. In the former and latter cases, the correlation functions exhibit the two-site and four-site periodicities, respectively. In two-dimensions, various spin-correlation functions are calculated up to the size of 4×4. The Néel-type spin correlation dominates at large values of J_0/J_2, while a 2×2 plaquette correlation is prominent at small values of this ratio. Between them, a columnar spin-Peierls dimerization correlation peaks. We infer the competition among the plaquette ordering, the dimer ordering, and the Néel ordering in the 2D system.

DOI: 10.1103/PhysRevB.84.054406 PACS number(s): 71.10.Fd, 75.10.Jm, 71.10.Pm, 75.40.Mg

I. INTRODUCTION

The recent experimental progress on the ultracold Fermi gases with large hyperfine spin provides an exciting opportunity to investigate novel physical properties.[1–4] In usual condensed-matter systems, large spin is not considered particularly interesting because large values of spin suppress quantum fluctuations. For example, in transition-metal oxides, a large spin on each cation site is usually referred as an effective spin S composed of $2S$ electrons by Hund's rule. The spin exchange between two cation sites at the leading order of the perturbation theory involves swapping only one pair of electrons, regardless of how large S is. The variation of S_z is only ± 1; thus increasing S reduces quantum fluctuations known as the $1/S$ effect. In contrast, in ultracold fermion systems, the situation is dramatically different, in which large hyperfine spin enhances quantum fluctuations. Each atom moves as a whole object carrying a large hyperfine spin. Exchanging cold fermions can completely flip the entire hyperfine-spin configuration, and thus enhances quantum fluctuations. In other words, large-spin physics in solid state systems is usually in the large-S limit, while in cold atom systems it is in the large-N limit, where N is the number of fermion components $2F + 1$.[3] We follow the convention in atomic physics to use F to denote the hyperfine spin of the atom.

Ultracold fermion systems with large hyperfine spins have aroused a great deal of theoretical interests. Early work studied the rich structures of the Fermi liquid theory[5] and the Cooper pairing structures.[6] Considerable progress has been made in the simplest large hyperfine-spin systems with $F = \frac{3}{2}$, whose possible candidate atoms are ^{132}Cs, ^{9}Be, ^{135}Ba, ^{137}Ba, and ^{201}Hg. These include both alkaline-earth-like atoms with zero electron spin due to the fully filled electron shells, and non-alkaline-earth atoms with nonzero electron spins.[4,7,8] In both cases, a generic $Sp(4)$, or, isomorphically, $SO(5)$, symmetry is proved without fine tuning. Such a high symmetry without fine-tuning is rare in both condensed matter and cold atom systems. It brings hidden degeneracy in the collective modes in the Fermi liquid theory,[9] fruitful patterns of quantum magnetism,[4,7,8,10,11] and Cooper pairing with large internal spin degrees of freedom.[8,12,13] Further investigations in the community include the study of Mott-insulating states,[14–19] Beth-ansatz solution,[20,21] Kondo effect,[22] and the four-fermion quartetting superfluidity.[23–25] Recently, $SU(N)$ models have been proposed for the alkaline-earth fermion atoms since their interactions are insensitive to their nuclear spins. It is a special case of the $Sp(N)$ model by further tuning interaction parameters of spin singlet and multiplet channels to be the same.[26–28] The possible ferromagnetic states have also been studied for the $SU(6)$ symmetric system of ^{173}Yb.[29] A detailed summary is presented in a review Ref. 4 and a nontechnique introduction is published at Ref. 3 by one of the authors. In a different context of heavy fermion systems, the effects of sympletic symmetry on quantum magnetism have also been studied in Ref. 30 and 31. The relations of the Haldane-gap in SU(N) spin chains and 2N-component fermionic systems with attractive interactions at half-filling have also been discussed.[32,33]

One-dimensional (1D) systems are important for the study of strong correlation physics because of the dominant interaction effects. Furthermore, controllable analytical and numeric methods are available. In Ref. 11, one of the authors performed the bosonization method to study competing phases in 1D systems with $F = \frac{3}{2}$, including the gapless Luttinger liquid, spin-gapped Luther–Emery liquid with Cooper pairing instability, and four-fermion quartetting superfluid at incommensurate fillings. At commensurate fillings with strong repulsive interactions, a charge gap opens and the systems become Mott insulating. The gapless Luttinger liquid phase becomes a gapless spin-liquid phase at quarter-filling and

 ©2011 American Physical Society

dimerized at half-filling, respectively.[4] The Luther–Emery phase becomes the gapped $Sp(4)$ dimer phase at quarter-filling and the on-site singlet phase at half-filling, respectively.[4]

On the other hand, the two-dimensional (2D) $Sp(4)$ Heisenberg model is still far away from clear understanding. Such a system can bring fruitful intriguing features of quantum magnetism which do not exhibit in usual solid state systems. For example, in the special case of the $SU(4)$ symmetry, four particles are required to form an $SU(4)$ singlet; thus its quantum magnetism is characterized by the four-site correlation beyond two sites. Such a state is the analogy to the three-quark color singlet baryon state in quantum chromodynamics. It is also the magnetism counterpart of the four-fermion quartetting instability with attractive interactions.[4] Recently a magnetic phase diagram in a spatially anisotropic square lattice of the $Sp(4)$ quantum magnetism is provided by means of large-N field-theoretical approach.[34] A phase transition between the long-range Néel order state and the disordered-valence-bond solid phase is discovered by the perturbative renormalization group equations. However, the model on an isotropic square lattice is still unexplored. In particular, quantum Monte Carlo (QMC) methods for this model suffer the notorious sign problem except in the special case where only the singlet bond exchange exists.

In this paper, we present a systematic numerical study for the $Sp(4)$ Heisenberg model at quarter filling in both 1D systems with large sizes and 2D systems up to 4×4 by means of exact diagonalization techniques and the density matrix renormalization group (DMRG).[35,36] In one dimension, we numerically show that the system exhibits two competing quantum phases: a long-range-ordered gapped dimer phase when the exchange interaction in the bond singlet channel (J_0) dominates over that in the quintet channel (J_2), and a gapless spin-liquid phase otherwise. The $Sp(4)$ spin-correlation functions are calculated, which show that in the dimer phase the correlations have the two-site periodicity, whereas in the gapless spin-liquid phase they have the four-site periodicity. In two dimensions, our numerical simulations for small sizes indicate three different dominant correlations depending on the values of J_0/J_2. We infer three competing phases: the Néel ordering, the plaquette ordering, and another possible phase of columnar dimer ordering, in the thermodynamic limit.

The rest of this paper is organized as follows. In Sec. II, we introduce the Hamiltonian of spin-3/2 fermions which possess the rigorous $Sp(4)$ symmetry and a magnetic exchange model in the Mott-insulating state at quarter-filling. A self-contained introduction of the $Sp(4)/SO(5)$ algebra is given. Then we separate our main discussion into two parts: Sec. III for 1D and Sec. IV for 2D systems. In Sec. III A, we study the low-energy spectra of a finite-size $Sp(4)$ chain with both open and periodic boundary conditions. In Sec. III B, the DMRG calculation on the spin-correlation functions are presented to identify the gapped $Sp(4)$ dimer phase and the gapless spin-liquid phase. In the second half, we first analyze the 2×2 cluster in Sec. IV A and we perform exact diagonalization on larger sizes to study the low-energy spectrum behavior in Sec. IV B. Then we display the calculations of the magnetic structure form factor in Sec. IV C, the dimer correlation in Sec. IV D, and the plaquette-type correlation in Sec. IV E. We discuss the possible existence of the corresponding orderings. Conclusions are made in the last section. At the end of this paper, we present a brief and self-contained introduction to the representation theory of Lie group in Appendices A–C.

II. MODEL HAMILTONIAN AND THE HIDDEN $Sp(4)$ SYMMETRY

A. The spin-3/2 Hubbard model

We start with the generic one-band Hubbard model loaded with spin-3/2 fermions. By neglecting long-range Coulomb interactions, only on-site interactions are considered in the Hubbard model. Due to Pauli's exclusion principle, the spin wave functions of two on-site fermions have to be antisymmetric. The total spin of two on-site spin-3/2 fermions can only be either singlet ($S_T = 0$) or quintet ($S_T = 2$). We assign an independent interaction parameter U_0 (singlet) and U_2 (quintet), respectively, to each channel. The Hamiltonian reads

$$H = -t \sum_{\langle ij\rangle,\sigma} (\psi^\dagger_{i\sigma}\psi_{j\sigma} + \text{h.c.}) - \mu \sum_{i\sigma} \psi^\dagger_{i\sigma}\psi_{i\sigma} + U_0 \sum_i P^\dagger_0(i)P_0(i) + U_2 \sum_{i,m=-2,..,2} P^\dagger_{2m}(i)P_{2m}(i), \quad (1)$$

where $\langle ij\rangle$ denotes the nearest-neighboring (NN) hopping; σ represents four spin flavors $F_z = \pm\frac{3}{2}, \pm\frac{1}{2}$ and $P^\dagger_0$ and $P^\dagger_{2,m}$ are the singlet and quintet pairing operators defined through Clebsch Gordon coefficients as

$$P^\dagger_0(i) = \sum_{\alpha\beta} \left\langle 00 \middle| \frac{3}{2}\frac{3}{2}\alpha\beta \right\rangle \psi^\dagger_\alpha(i)\psi^\dagger_\beta(i),$$
$$P^\dagger_{2m}(i) = \sum_{\alpha\beta} \left\langle 2m \middle| \frac{3}{2}\frac{3}{2}\alpha\beta \right\rangle \psi^\dagger_\alpha(i)\psi^\dagger_\beta(i). \quad (2)$$

The actual symmetry of Eq. (1) is much larger than the $SU(2)$ symmetry: It has a hidden and exact $Sp(4)$, or, isomorphically, $SO(5)$ symmetry. The $Sp(4)$ algebra can be constructed as follows. For the four-component fermions, there exist 16 bases for the 4×4 Hermitian matrices $M_{\alpha\beta}(\alpha,\beta = \pm\frac{3}{2}, \pm\frac{1}{2})$. They serve as matrix kernels for the bilinear operators, i.e., $\psi^\dagger_\alpha M_{\alpha\beta}\psi_\beta$, in the particle-hole channel. The density and three-component spin F_x, F_y, F_z operators *do not* form a complete set. The other 12 operators are built up as high-rank spin tensors, including five-component spin-quadrupoles and seven-component spin-octupoles. The matrix kernels of the spin-quadrupole operators are defined as

$$\Gamma^1 = \frac{1}{\sqrt{3}}(F_xF_y + F_yF_x), \quad \Gamma^2 = \frac{1}{\sqrt{3}}(F_zF_x + F_xF_z),$$
$$\Gamma^3 = \frac{1}{\sqrt{3}}(F_zF_y + F_yF_z), \quad \Gamma^4 = \left(F_z^2 - \frac{5}{4}\right), \quad (3)$$
$$\Gamma^5 = \frac{1}{\sqrt{3}}\left(F_x^2 - F_y^2\right),$$

which anticommute with each other and thus form a basis of the Dirac-Γ matrices. The matrix kernels of three spin and seven spin-octupole operators together are generated from the commutation relations among the five Γ matrices as

$$\Gamma^{ab} = -\frac{i}{2}[\Gamma^a, \Gamma^b] \quad (1 \leqslant a,b \leqslant 5). \quad (4)$$

Consequently, these 16 bilinears can be classified as

$$n = \psi_\alpha^\dagger \psi_\alpha, n_a = \tfrac{1}{2}\psi_\alpha^\dagger \Gamma^a_{\alpha\beta}\psi_\beta, \quad L_{ab} = -\tfrac{1}{2}\psi_\alpha^\dagger \Gamma^{ab}_{\alpha\beta}\psi_\beta, \qquad (5)$$

where n is the density operator; n_a's are five-component spin-quadrupole operators; L_{ab}'s are 10-component spin and spin-octupole operators.[4,10] Reversely the spin $SU(2)$ generators $F_{x,y,z}$ can be written as $F_+ = \sqrt{3}(-L_{34} + iL_{24}) - (L_{12} + iL_{25}) + i(L_{13} + iL_{35})$ and $F_z = L_{23} + 2L_{15}$.

The 15 operators of n_a and L_{ab} together span the $SU(4)$ algebra. Among them, the 10 L_{ab} operators are spin tensors with odd ranks, and thus time-reversal (TR) odd, while the five-component n_a's are TR even. The TR odd operators of L_{ab} form a closed subalgebra of $Sp(4)$. The four-component spin-3/2 fermions form the fundamental spinor representation of the $Sp(4)$ group. In contrast, the TR even operators of n_a do not form a closed algebra, but transform as a five-vector under the $Sp(4)$ group. In other words, $Sp(4)$ is isomorphic to $SO(5)$. But, rigorously speaking, the fermion spinor representations of $Sp(4)$ are not representations of $SO(5)$. Their relation is the same as that between $SU(2)$ and $SO(3)$. Below we will use the terms of $Sp(4)$ and $SO(5)$ interchangeably. The $SO(5)$ symmetry of Eq. (1) can be intuitively understood as follows. The four-component fermions are equivalent to each other in the kinetic energy term, which has an obvious $SU(4)$ symmetry. Interactions break the $SU(4)$ symmetry down to $SO(5)$. The singlet and quintet channels form the identity and five-dimensional vector representations for the $SO(5)$ group, respectively; thus Eq. (1) is $SO(5)$ invariant without any fine-tuning.

B. Magnetic exchanges at quarter-filling

Mott-insulating states appear at commensurate fillings with strong repulsive interactions. We focus on the magnetic exchange at quarter filling, i.e., one fermion per site. The Heisenberg-type exchange model has been constructed in Ref. 7 through the second-order perturbation theory. For each bond, the exchange energies are $J_0 = \frac{4t^2}{U_0}$ for the bond spin-singlet channel, $J_2 = \frac{4t^2}{U_2}$ for the bond spin-quintet channel, and $J_1 = J_3 = 0$ for the bond spin-triplet and septet channels, respectively. This exchange model can be written in terms of bilinear, biquadratic, and bicubic Heisenberg exchange, and the Hamiltonian reads as

$$H_{ex} = \sum_{\langle i,j\rangle} a(\vec{F}_i \cdot \vec{F}_j) + b(\vec{F}_i \cdot \vec{F}_j)^2 + c(\vec{F}_i \cdot \vec{F}_j)^3, \qquad (6)$$

where $a = -\frac{1}{96}(31J_0 + 23J_2)$, $b = \frac{1}{72}(5J_0 + 17J_2)$, and $c = \frac{1}{18}(J_0 + J_2)$, and $F_{x,y,z}$ are usual 4×4 spin operators. Equation (6) can be simplified into a more elegant form with the explicitly $SO(5)$ symmetry[4] as

$$H_{ex} = \sum_{\langle i,j\rangle} \left\{ \sum_{1\leqslant a<b\leqslant 5} \frac{J_0 + J_2}{4} L_{ab}(i)L_{ab}(j) + \frac{3J_2 - J_0}{4} \sum_{a=1}^{5} n_a(i)n_a(j) \right\}. \qquad (7)$$

In the $SO(5)$ language, there are two diagonal operators commuting with each other and read as

$$L_{15} = \tfrac{1}{2}\left(n_{\frac{3}{2}} + n_{\frac{1}{2}} - n_{-\frac{1}{2}} - n_{-\frac{3}{2}}\right),$$
$$L_{23} = \tfrac{1}{2}\left(n_{\frac{3}{2}} - n_{\frac{1}{2}} + n_{-\frac{1}{2}} - n_{-\frac{3}{2}}\right). \qquad (8)$$

Corresponding to the spin language, each singlet-site basis state can be labeled in terms of these two quantum numbers as $|F_z\rangle = |L_{15}, L_{23}\rangle$: $|\pm\frac{3}{2}\rangle = |\pm\frac{1}{2}, \pm\frac{1}{2}\rangle$ and $|\pm\frac{1}{2}\rangle = |\pm\frac{1}{2}, \mp\frac{1}{2}\rangle$. For an arbitrary many-body state, $L_{15}^{tot} = \sum_i L_{15}(i)$ and $L_{23}^{tot} = \sum_i L_{23}(i)$ are good quantum numbers [similar to that, $F_z^{tot} = \sum_i F_z(i)$ is conserved in $SU(2)$ cases] and can be applied to reduce dimensions of the Hilbert space in practical numerical calculations.

There exist two different $SU(4)$ symmetries of Eq. (7) in two special cases. At $J_0 = J_2 = J$, i.e., $U_0 = U_2$, it reduces to the $SU(4)$ Heisenberg model with each site in the fundamental representation

$$H = \sum_{\langle i,j\rangle} \frac{J}{2}\{L_{ab}(i)L_{ab}(j) + n_a(i)n_a(j)\}. \qquad (9)$$

Below we denote this symmetry as $SU(4)_A$. In this case, there is an additional good quantum number n_4,

$$n_4 = \tfrac{1}{2}\left(n_{\frac{3}{2}} - n_{\frac{1}{2}} - n_{-\frac{1}{2}} + n_{-\frac{3}{2}}\right). \qquad (10)$$

This $SU(4)$ model is equivalent to the Kugel–Khomskii-type model[37,38] and is used to study the physics with interplay between orbital and spin degrees of freedom.[39–41] On the other hand, at $J_2 = 0$, i.e., $U_2 \to +\infty$, Eq. (7) has another $SU(4)$ symmetry in the bipartite lattice, which is denoted as $SU(4)_B$ below. In this case, we perform the particle-hole transformation to one sublattice but leave the other sublattice unchanged. The particle-hole transformation is defined as $\psi_\alpha \to R_{\alpha\beta}\psi_\beta^\dagger$, where R is the charge conjugation matrix

$$R = \begin{pmatrix} 0 & i\sigma_2 \\ i\sigma_2 & 0 \end{pmatrix}. \qquad (11)$$

Under this operation, the fundamental representation transforms to an antifundamental representation whose $Sp(4)$ generators and vectors become $L'_{ab} = L_{ab}$ and $n'_a = -n_a$. Thus Eq. (7) can be recast to

$$H = \sum_{\langle i,j\rangle} \frac{J}{2}(L'_{ab}(i)L_{ab}(j) + n'_a(i)n_a(j)), \qquad (12)$$

which is $SU(4)$ invariant again.

These two $SU(4)$ symmetries have very different physical properties. In the case of $SU(4)_A$, two sites are not enough to form an $SU(4)$ singlet. It needs at least four sites to form an $SU(4)$ singlet as $\epsilon_{\alpha\beta\gamma\delta}\psi_\alpha^\dagger(1)\psi_\beta^\dagger(2)\psi_\gamma^\dagger(3)\psi_\delta^\dagger(4)$, where $\epsilon_{\alpha\beta\gamma\delta}$ is the rank-four fully antisymmetric tensor. Thus the quantum magnetism of Eq. (7) at $J_0 = J_2$ is characterized by four-site correlations. The ground state (GS) of such a system on a 2D square lattice was conjectured to be a plaquette $SU(4)$ singlet state without magnetic long-ranged ordering.[40,42] On the other hand, for the $SU(4)_B$ case, two sites can form an $SU(4)$ singlet as $R_{\alpha\beta}\psi_\alpha^\dagger(1)\psi_\beta^\dagger(2)$. In the 2D square lattice, a long-ranged Néel order is identified by QMC simulations[43] and large-N limit.[44] The square of the staggered magnetization is numerically given

as $m_s = 0.091$, which is much smaller than that of the $SU(2)$ Néel order state.

III. QUANTUM MAGNETISM IN THE 1D CHAINS

We start our discussion on the 1D chain. The phase diagram of the 1D spin-3/2 Hubbard model has been studied by one of the authors using the method of bosonization.[4,11] At the commensurate quarter-filling (one particle per site) with purely repulsive interactions ($U_0 > 0, U_2 > 0$), the $4k_f$-Umklapp term opens a charge gap as $K_c < \frac{1}{2}$. In this case, the physics is captured by the exchange model of Eq. (7). It has been found that in the regime of $J_0/J_2 > 1$ dimerization of spin Perierls order is present, whereas it is a gapless spin-liquid phase at $J_0/J_2 \leqslant 1$ (see Fig. 1).[11] In the following, we use exact diagonalization methods and DMRG not only to identify these two competing phases but also to demonstrate the G5 profiles and four-site periodicities in spin-spin correlations.

A. Exact diagonalization on low-energy spectra

In this subsection, we apply the exact diagonalization technique to study the 1D $Sp(4)$ spin-3/2 chains with NN exchange interactions described by Eq. (7). We consider only the case of the site number $N = 4m$. For convenience, we set $J_0 = \sqrt{2}\sin\theta$ and $J_2 = \sqrt{2}\cos\theta$. Regardless of θ and sizes N, the GS, exist only in the $(L_{15}^{tot}, L_{23}^{tot}) = (0,0)$ sector and are unique with $C = 0$, where C denotes the $Sp(4)$ Casimir of the entire system and is expressed in terms of the $Sp(4)$ generators as

$$C = \sum_{1\leqslant a<b\leqslant 5} \left\{ \sum_i L_{ab}(i) \right\}^2. \tag{13}$$

In addition to L_{15}^{tot} and L_{23}^{tot}, the Casimir C is also a conserved quantity in the $Sp(4)$ system, analogous to the total spin in $SU(2)$ systems. Each energy eigenstate can be labeled by C and further identifies the dimension of the representation (degeneracy). As shown in table II in Appendix B, while $C = 0$, the state is an $Sp(4)$ singlet and unique whereas as

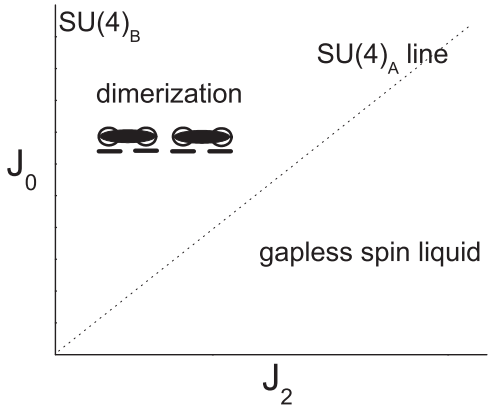

FIG. 1. Phase diagram of the 1D chain in terms of the singlet and quintet channel interaction J_0 and J_2. In this context, θ is the angle defined by $\theta = \tan^{-1}(J_0/J_2)$. The $SU(4)_A$ type ($\theta = 45^\circ$) denoted by the dotted line belongs to the gapless spin-liquid state whereas $SU(4)_B$ is along $J_2 = 0$. The phase boundary separating the dimerization phase and the gapless liquid state is the $SU(4)_A$ line.

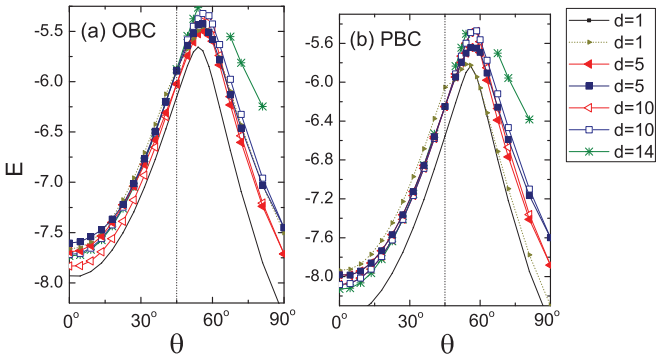

FIG. 2. (Color online) The exact diagonalization on a 1D chain with 12 sites for (a) open and (b) periodic boundary conditions. The dispersion of the (GS) and low excited states and the dimensions d of their corresponding representations of the $Sp(4)$ group are shown.

$C > 0$ the state is multiplet and has degeneracy which is equal to the dimension of the associated representation.

In Fig. 2(a) and 2(b), the GS and low excited states (LESs) with 12 sites are presented using open and periodic boundary conditions, respectively. The GS as varying θ angles is always an $Sp(4)$ singlet, which becomes an $SU(4)$ singlet at $\theta = 45^\circ$ $[SU(4)_A]$ and $\theta = 90^\circ$ $[SU(4)_B]$ for both boundary conditions. For the low-energy excited states, we first look at the regime of $45^\circ < \theta < 90^\circ$, i.e., $J_0 > J_2$. With open boundary conditions (OBCs), the LESs are the $Sp(4)$ five-vector states with the quadratic Casimir $C = 4$. The next-lowest excited states (NLESs) are 10-fold degenerate and belong to the 10-dimensional (10d) $Sp(4)$ adjoint representation with $C = 6$. The LES and NLES merge at both of the $SU(4)_A(\theta = 45^\circ)$ and $SU(4)_B(\theta = 90^\circ)$ points, and become 15-fold degenerate. This is the $SU(4)$ adjoint representation with $C = 8$. With periodic boundary conditions (PBCs), the five-vector and the 10-fold states behave similarly as before. However, a marked difference is that a new $Sp(4)$ singlet state appears as the LES at $50^\circ < \theta < 90^\circ$, which becomes higher than the five-vector states only very close to 45°. In particular, it is nearly degenerate with the GS [which is the lowest $Sp(4)$ singlet] at $\theta = 50^\circ \sim 60^\circ$. In the regime of $0^\circ < \theta < 45^\circ$, i.e., $J_2 > J_0$ the excited states are many $Sp(4)$ multiplets with energies close to each other. With OBCs, the LESs form the 10d $Sp(4)$ adjoint representation. For the PBC case, the 14-dimensional symmetric tensor representation of $Sp(4)$ competes with the 10d adjoint one.

The appearance of two nearly degenerate $Sp(4)$ singlets at $50^\circ < \theta < 90^\circ$ with PBCs and their disappearance with OBCs can be understood by the dimerization instability. The dimerization and the spin-gapped GS was shown in the bosonization analysis at $45^\circ < \theta < 90^\circ$.[11] In the thermodynamic limit, the GS has double degeneracy corresponding to two different dimer configurations, both spontaneously breaking translational symmetry. The OBC favors only one of the dimer configurations, but disfavors the other due to one bond breaking. In the finite system with the PBC, the two dimer configurations tunnel between each other, which gives rise to two nearly degenerate $Sp(4)$ singlet states. We further calculate the gap between them, denoted by Δ_{ss}, at $\theta > 45^\circ$, by using exact diagonalization under PBC up to 16 sites.

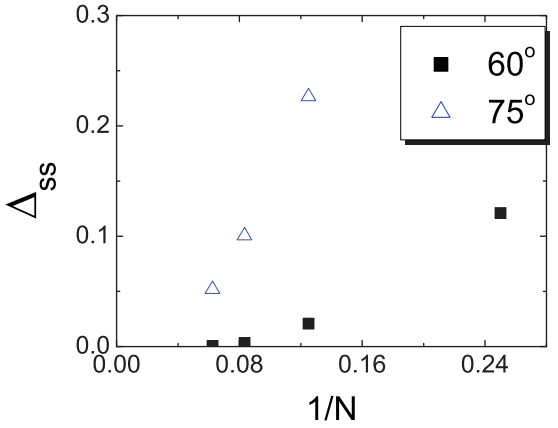

FIG. 3. (Color online) Exact diagonalization results on the $Sp(4)$ singlet-singlet gap with $J_0 > J_2$ and periodic boundary conditions ($\theta = 60^\circ$ and 75° with $N = 8,12$ and 16). Finite size scaling shows the vanishing of the singlet-singlet gap Δ_{ss}.

As presented in Fig. 3, Δ_{ss} disappears in the finite-size scaling due to the twofold degeneracy. On the other hand, the existence of the spin gap in this parameter regime is presented in Fig. 4 by DMRG simulation in Sec. III B below. The original Lieb–Schultz–Mattis theorem[45] was proved that, for the $SU(2)$ case, the GS of half-integer spin chains with translational and rotational symmetries is gapless, or gapped with breaking translational symmetry. It is interesting to observe that our results of the $Sp(4)$ spin chain also agree with this theorem. The nature of the GS in the parameter regime $0^\circ < \theta < 45^\circ$ will be discussed in Sec. III B.

B. DMRG simulations on $Sp(4)$ spin chain

In this subsection, we present the DMRG calculations on the GS properties of the $Sp(4)$ chain up to 80 sites with OBC. We first present the spin gap Δ_{sp} in Fig. 4, which is defined as the energy difference between the GS and the lowest $Sp(4)$ multiplet.

For chains with an even number of sites, the GS is obtained with quantum number $L_{15}^{tot} = L_{23}^{tot} = 0$, and any $Sp(4)$ multiplet contains the states with quantum numbers $(L_{15}^{tot} = \pm 1, L_{23}^{tot} = 0)$ and $(L_{15}^{tot} = 0, L_{23}^{tot} = \pm 1)$. States with the same values of $(L_{15}^{tot}, L_{23}^{tot})$ may belong to different $Sp(4)$ representations, which can be distinguished by their $Sp(4)$ Casimir. Practically, we need to calculate only these sectors with low integer values of $(L_{15}^{tot}, L_{23}^{tot})$ to determine the spin gaps. For the cases of $\theta > 45^\circ$, i.e., $(J_2/J_0 < 1)$, Δ_{sp}'s saturate to nonzero values as $1/N \to 0$, indicating the opening of spin gaps. On the other hand, Δ_{sp}'s vanish at $\theta \leqslant 45^\circ$, which shows that the GS is gapless. These results agree with the bosonization analysis,[11] which shows that the phase boundary is at $\theta = 45^\circ$ with the $SU(4)_A$ symmetry, which is also gapless. This gapless $SU(4)_A$ line was also studied before in Refs. 46 and 47.

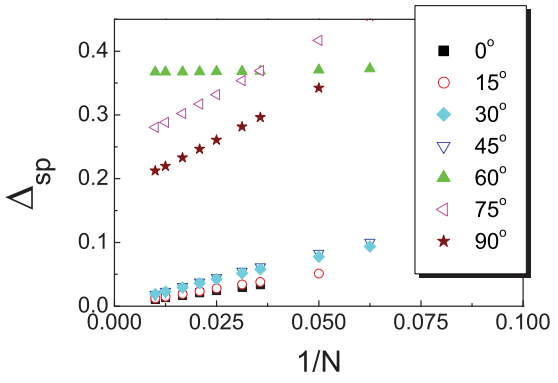

FIG. 4. (Color online) The finite-size scaling of the spin gap Δ_{sp} of the $Sp(4)$ spin chain vs. $1/N$ at various values of θ. θ is defined as $\theta = \tan^{-1}(J_0/J_2)$ and N is the system size.

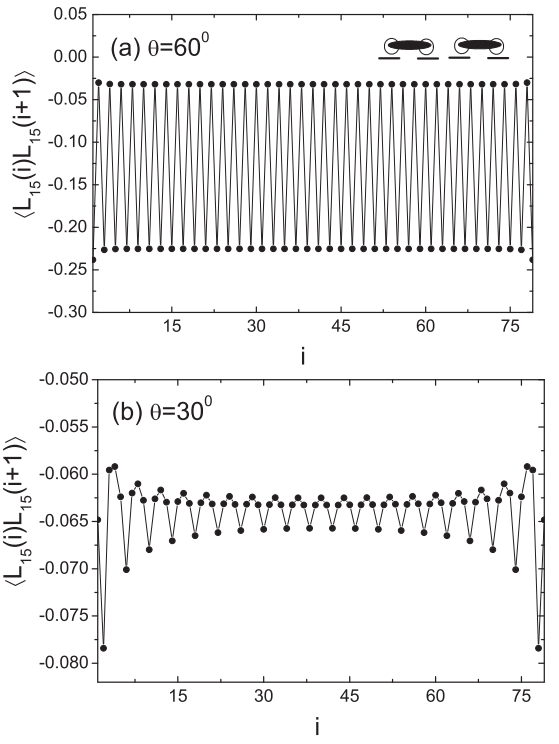

FIG. 5. The NN correlation of $\langle L_{15}(i)L_{15}(i+1)\rangle$ with OBCs for (a) $\theta = 60^\circ$ and (b) $\theta = 30^\circ$, respectively. The dimer ordering is long ranged in (a). Note the two-site periodicity in (a) and the four-site periodicity in (b).

To further explore the GS profile, we calculate the NN correlation functions of the $Sp(4)$ generators for a chain of 80 sites. This correlation function is similar to the bonding strength and defined as $\langle X(i)X(i+1)\rangle$, where X are $Sp(4)$ generators. We present the result of $\langle L_{15}(i)L_{15}(i+1)\rangle$ in Fig. 5, and the correlation functions of other generators should be the same due to the $Sp(4)$ symmetry. The open boundary induces characteristic oscillations. At $\theta = 60^\circ$, i.e., $J_0/J_2 = \sqrt{3}$, $\langle L_{15}(i)L_{15}(i+1)\rangle$ exhibits the dominant dimer pattern, which does not show noticeable decay from the edge to the middle of the chain. This means that the dimerization is long-range ordered in agreement with the bosonization analysis.[4] In contrast, at $\theta^\circ = 30^\circ$, i.e., $J_2/J_0 = \sqrt{3}$, $\langle L_{15}(i)L_{15}(i+1)\rangle$ exhibits a characteristic power-law decay with four-site periodicity oscillations. The four-site periodicity is also observed at other θ's for $\theta \leqslant 45^\circ$, the same as the ones presented in the bosonization analysis.

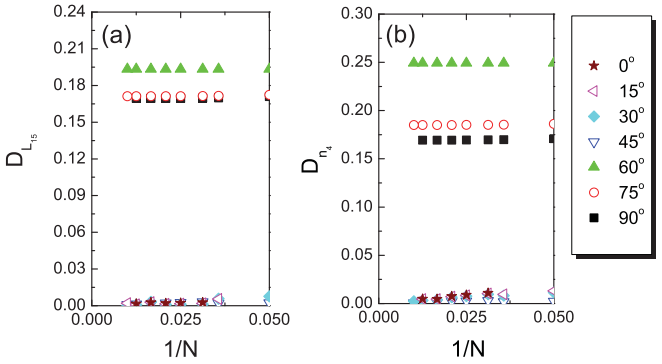

FIG. 6. (Color online) The finite-size scaling for the dimer order parameters (a) $D_{L_{15}}$ and (b) D_{n_4} vs. $1/N$ at various θ's.

We follow the definition for the dimer order parameter in Refs. 48 and 49 as

$$D_X = \left|\left\langle X\left(\frac{N}{2}-1\right)X\left(\frac{N}{2}\right)\right\rangle - \left\langle X\left(\frac{N}{2}\right)X\left(\frac{N}{2}+1\right)\right\rangle\right|. \quad (14)$$

As shown previously, X's are $Sp(4)$ generators and vectors in the $Sp(4)$ spin chain. Without loss of generality, we choose two nonequivalent operators as $X = L_{15}$ and n_4 for $Sp(4)$ generators and vectors, respectively. The OBCs provide an external field to pin down the dimer orders. The finite-size scaling of the dimer orders of the two middle bonds is presented in Figs. 6(a) and 6(b) at various values of θ, respectively. It is evident that in the regime of $\theta > 45^\circ$ both $D_{L_{15}}$ and D_{n_4} remain finite as $1/N \to 0$, whereas for $\theta \leqslant 45^\circ$ the dimer order parameters vanish. We conclude that the GS is the dimer phase for $J_0/J_2 > 1$.

Next we present the two point correlation functions of $\langle X(i)X(j)\rangle$, where X is L_{15} and n_4, in Figs. 7(a) and 7(b), respectively. At $\theta > 45^\circ$, say, $\theta = 60^\circ$, both correlation functions show exponential decay due to the dimerization. In the spin-liquid regime of $\theta \leqslant 45^\circ$, i.e., $J_2 \geqslant J_0$, however, all the correlation functions exhibit the power-law behavior and the same $2k_f$ oscillations with the four-site period. Their asymptotic behavior can be written as

$$\langle X(i_0)X(i)\rangle \propto \frac{\cos\frac{\pi}{2}|i-i_0|}{|i-i_0|^\kappa}. \quad (15)$$

Along the $SU(4)_A$ line ($\theta = 45^\circ$), the correlations of L_{15} and n_4 are degenerate. The power can be fitted as $\kappa \approx 1.52$, which is in good agreement with the value of 1.5 from bosonization analysis and numerical studies.[11,46,47,50] As θ is away from 45°, the $SU(4)$ symmetry is broken. For the correlations of L_{15}, the values of κ decrease as decreasing θ, which can be fitted as $\kappa = 1.41, 1.34, 1.30$ for $\theta = 30^\circ, 15^\circ, 0^\circ$, respectively. On the other hand, for the correlations of n_4, the values of κ can be fitted as $\kappa = 1.55, 1.65, 1.60$ for $\theta = 30^\circ, 15^\circ, 0^\circ$, respectively. We also perform the Fourier transforms of the correlations of $\langle L_{15}(i_0)L_{15}(i)\rangle$, $S(q)$, and present the results in the inset of Fig. 7(a). $S(q)$ is defined as

$$S(q) = \sum_{i,j} e^{iq(r_i - r_j)}\langle L_{15}(r_i)L_{15}(r_j)\rangle \quad (16)$$

and $q = m\pi/(N+1)$, where $m = 1, 2, \ldots, N$ are integers for the OBC. Clearly, in the regime of $\theta \leqslant 45^\circ$ all the peaks are

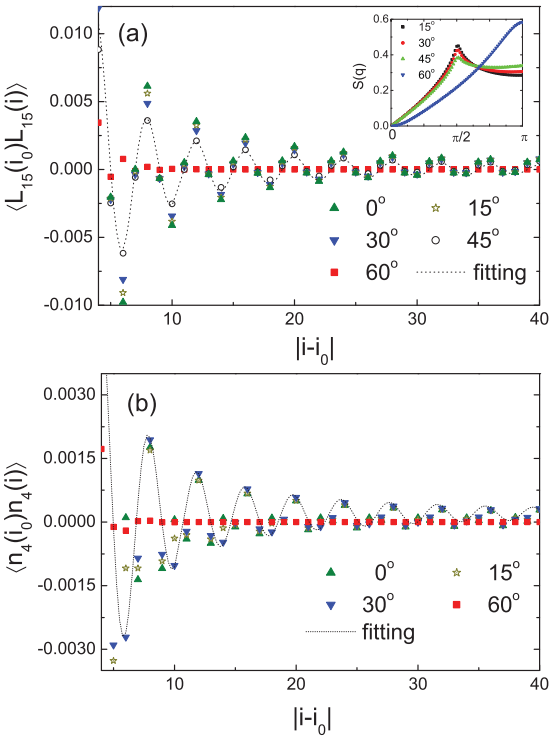

FIG. 7. (Color online) (a) The two point correlations $\langle L_{15}(i_0)L_{15}(i)\rangle$ at $\theta = 0^\circ, 15^\circ, 30^\circ, 45^\circ$, and 60°. The dotted line is plotted by the fitting result using $\cos(x\pi/2)/x$.[1.52] The reference point i_0 (=40) is the most middle site of the chain ($N = 80$). The inset indicates that all $S(q)$ for $\theta \leqslant 45^\circ$ have peaks located at $q = 41\pi/81 \sim \pi/2$ whereas π for $\theta = 60^\circ$. (b) $\langle n_4(i_0)n_4(i)\rangle$ at $\theta = 0^\circ$, 15°, 30°, and 60° and the fitting uses $\kappa = 1.55$.

located at $q = 41\pi/81 \sim \pi/2$, indicating a $2k_f$ charge density wave. On the other hand, $S(q)$ at $\theta = 60^\circ$ appears a peak at π, which denotes a $4k_f$ charge density wave and is characteristic of the dimerization phase.

IV. THE $Sp(4)$ MAGNETISM IN 2D SQUARE LATTICE WITH SMALL SIZES

The quantum magnetism of Eq. (7) in two dimensions is a very challenging problem. Up to now, a systematic study is still void. In the special case of the $SU(4)_B$ line, i.e. $J_2 = 0$, in the square lattice, QMC simulations are free of the sign problem, which shows the long-range-Néel ordering but with very small Néel moments $n_4 = (-)^i L_{15} = (-)^i L_{23} \approx 0.05$.[43] This result agrees with the previous large-N analysis.[51] The Goldstone manifold is $CP(3) = U(4)/[U(1) \otimes U(3)]$ with six branches of spin waves. On the other hand, on the $SU(4)_A$ line with $J_0 = J_2$, an exact diagonalization study on the 4×4 sites shows the evidence of the four-site $SU(4)$ singlet plaquette ordering.[40] Large-size simulations are too difficult to confirm this result. On the other hand, a variational wave-function method based on the Majorana representation of spin operators suggests a spin-liquid state at the $SU(4)_A$ line.[52] Recently, Chen *et al.*[7] constructed an $SU(4)$ Majumdar–Ghosh model in a two-leg spin-3/2 ladder whose GS is solvable exhibiting this plaquette state. Exact models for trimerization and tetramerization in spin chains and a similar SU(3) plaquette state in a 2D

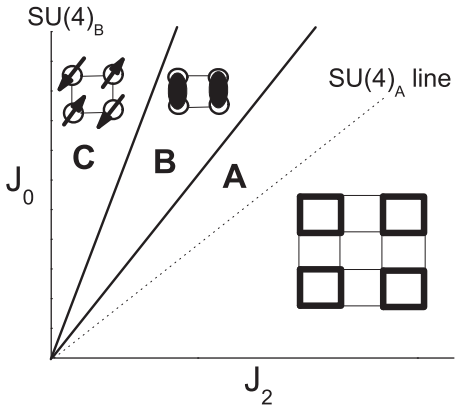

FIG. 8. Speculated phase diagram of the 2D $Sp(4)$ spin-3/2 systems at quarter filling from Ref. 4. $\theta = \tan^{-1}(J_0/J_2)$. The $SU(4)_A$ type drawn by the dotted line is at $J_0 = J_2$ ($\theta = 45^\circ$) whereas $SU(4)_B$ at $J_2 = 0$ ($\theta = 90^\circ$). Bold letters **A**, **B**, and **C** represent the plaquette, columnar dimerized, and Néel-order states, respectively.

frustrated Spin-1 model have been proposed in Ref. 53 and 54, respectively. An $SU(4)$ resonant plaquette model in three dimensions have also been constructed.[8,55]

Based on this available knowledge, a speculated phase diagram was provided in Ref. 4 and is shown in Fig. 8. The Néel-order state **C** is expected to extend to a region with finite J_2 instead of only along the $J_2 = 0$ line. Furthermore, the plaquette order phase **A** exists not only along the $SU(4)_A$ line but also covers a finite range including $\theta = 45^\circ$. Between **A** and **C**, there exists an intermediate phase **B** which renders ordered dimerizations which are two-sites spin singlets. However, these features have not been tested due to the lack of controllable analytic and numeric methods for 2D strongly correlation systems. For example, QMC methods suffer notorious sign problems at $J_2 \neq 0$.

In this section, we begin with the cluster of 2×2 whose GSs can be solved analytically. Then we perform exact diagonalization (ED) methods for the case of 4×4 sites and analyze the associated GS profiles for different values of θ. Even though the size that we are studying is still too small to draw any conclusion for the thermodynamic limit, it provides valuable information on the GS properties.

A. The 2 × 2 cluster

We begin with the 2×2 cluster, whose GS can be solved analytically for all the values of θ. Such a system contains three $Sp(4)$ singlets, and the GSs can be expanded in this singlet subspace. These $Sp(4)$ singlets can be conveniently represented in terms of the dimer states with the horizontal, vertical, and cross-diagonal configurations depicted in Fig. 9(a) as

$$\begin{aligned} |H\rangle &= \tfrac{1}{4} R_{\alpha\beta}\psi^\dagger_\alpha(4)\psi^\dagger_\beta(1)R_{\gamma\delta}\psi^\dagger_\gamma(2)\psi^\dagger_\delta(3)|\Omega\rangle, \\ |V\rangle &= \tfrac{1}{4} R_{\alpha\beta}\psi^\dagger_\alpha(1)\psi^\dagger_\beta(2)R_{\gamma\delta}\psi^\dagger_\gamma(3)\psi^\dagger_\delta(4)|\Omega\rangle, \\ |C\rangle &= \tfrac{1}{4} R_{\alpha\beta}\psi^\dagger_\alpha(1)\psi^\dagger_\beta(3)R_{\gamma\delta}\psi^\dagger_\gamma(2)\psi^\dagger_\delta(4)|\Omega\rangle, \end{aligned} \tag{17}$$

where R is the charge conjugation matrix defined in Eq. (11). These states are linearly independent but are not orthogonal to each other, satisfying $\langle H|V\rangle = \langle V|C\rangle = \langle C|H\rangle = -\frac{1}{4}$.

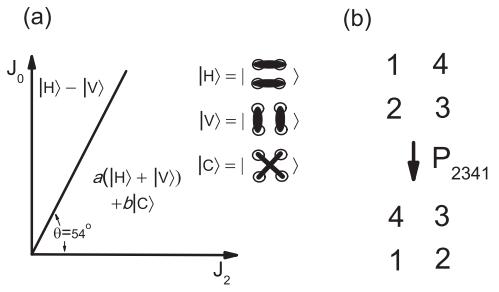

FIG. 9. (a) The GS wave functions of the 2×2 cluster at various θ. a and b are coefficients depending on θ and the thick bonds denote the two-site $Sp(4)$ spin singlet states. (b) The position indices before and after the permutation P_{2341}.

Under the permutation of the four sites $P_{(2341)}$, or a rotation at 90° as shown in Fig. 9(b), they transform as

$$P_{2341}|H\rangle = |V\rangle, \quad P_{2341}|V\rangle = |H\rangle, \quad P_{2341}|C\rangle = |C\rangle. \tag{18}$$

At $\theta = 45^\circ$, i.e., the $SU(4)_A$ case, the GS is exactly an $SU(4)$ singlet over the sites $1-4$:[7,39]

$$\left|\Psi^s_{SU(4)}\right\rangle = \frac{1}{\sqrt{4!}} \sum_{\mu\nu\tau\xi} \varepsilon_{\mu\nu\tau\xi}\psi^\dagger_{\mu,1}\psi^\dagger_{\nu,2}\psi^\dagger_{\tau,3}\psi^\dagger_{\xi,4}|\Omega\rangle, \tag{19}$$

where the indices μ,ν,τ,ξ run over $\pm\frac{3}{2}, \pm\frac{1}{2}$; $|\Omega\rangle$ represents the vacuum state; $\varepsilon_{\mu\nu\tau\xi}$ is a rank-four fully antisymmetric tensor. It can also be represented as the linear combination of the dimer states as

$$\left|\Psi^s_{SU(4)}\right\rangle = \sqrt{\frac{2}{3}}(|H\rangle + |V\rangle + |C\rangle), \tag{20}$$

which is even under the rotation operation P_{2341}. We find that, in the entire range of $0 \leqslant \theta < 54^\circ$, the GS wave functions remain even under such a rotation P_{2341}, whose wave functions can be represented as

$$|\Psi\rangle = a(|H\rangle + |V\rangle) + b|C\rangle, \tag{21}$$

where a and b are coefficients depending on the values of θ. In fact, the overlaps between GS wave functions, Eq. (21), and the $SU(4)$ singlet state $|\Psi_{SU(4)}\rangle$ are larger than 0.98 at $\theta < 54^\circ$. At $\theta > 54^\circ$, a level crossing occurs and the GS wave function changes to

$$\left|\Psi^s_{SU(4)}\right\rangle = \sqrt{\frac{2}{3}}\Big(|H\rangle - |V\rangle\Big), \tag{22}$$

which is independent of θ and odd under the rotation P_{2341}.

Combining the above observations, we identify that there are two competing states in the system. The boundary is located at $\theta = 54^\circ$. Next we turn to analyze large-size systems.

B. The low-energy spectra for the 4 × 4 cluster

In this subsection we study a larger system size of $N = 4 \times 4$. Both $L^{tot}_{15} = \sum_i L_{15}(i)$ and $L^{tot}_{23} = \sum_i L_{23}(i)$ are good quantum numbers, which can be used to reduce the Hilbert space. The dimension of the Hilbert space in the $(L^{tot}_{15}, L^{tot}_{23}) = (0,0)$ sector goes up to 165 million. On the other hand, the lowest multiplet states are located in the sector of $(L^{tot}_{15}, L^{tot}_{23}) = (0, \pm 1)$ or $(\pm 1, 0)$ and the corresponding dimension is about 147 million. The dimensions of the subspace are too large to

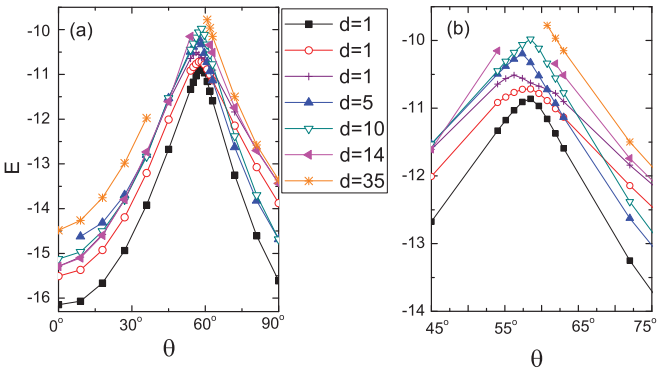

FIG. 10. (Color online) (a) The low-lying states for the 4×4 cluster at various values of θ. The dimensions of the corresponding $Sp(4)$ representations d are marked. The GS wave functions are always $Sp(4)$ singlets. (b) The zooming-in around $\theta \approx 63^\circ$ exhibiting various energy level crossings.

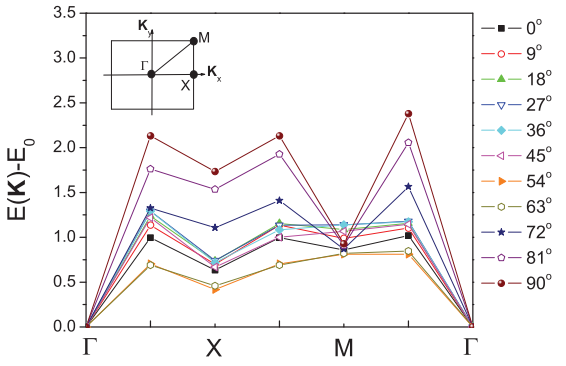

FIG. 11. (Color online) The energy dispersion $E(\vec{K}) - E_0$ vs. θ for the 4×4 cluster. Γ, M,X are the high symmetry points for the many-body GS momenta, corresponding to $\vec{K} = (0,0)$, (π,π), and $(\pi,0)$ respectively, in the first Brillouin zone.

perform diagonalization. Nevertheless, by using translational symmetry, the dimension of the Hilbert space reduces to 10 million such that ED calculations become doable. The GSs are always in the sector of total momentum $\vec{K} = (0,0)$ and are $Sp(4)$ singlets. In the following, except for the specific mention in Sec. IV E, the systems are considered under PBCs.

The low-lying energy spectra for the $N = 4 \times 4$ clusters for $0 < \theta < 90^\circ$ are displayed in Fig. 10. The GSs for all the values of θ are $Sp(4)$ singlets with Casimir $C = 0$, and that at $\theta = 45^\circ$ is an $SU(4)$ singlet. The LESs are also $Sp(4)$ singlet states at $\theta < 63^\circ$. The lowest spin multiplets appear as the 14-fold degenerate $Sp(4)$ symmetric tensor states with $C = 10$. A level crossing of the LESs appears around $\theta = 63^\circ$ implying that there exists competing phases nearby. At $\theta > 63^\circ$, the lowest excited states become five-fold degenerate $Sp(4)$ vector states with the Casimir $C = 4$. Another 10-fold degenerate state, which forms the $Sp(4)$ adjoint representation with $C = 10$, appear as the NLES. At the $SU(4)_B$ line, i.e., $\theta = 90^\circ$, these two sectors merge into the 15-fold degenerate states forming the adjoint representation of the $SU(4)$ group whose $SU(4)$ Casimir is $C = 8$.

In Sec. III A, the appearance of the $Sp(4)$ singlet as the LESs in the small-size systems implies the dimerization in the thermodynamic limit. This is confirmed in the large size DMRG results in Sec. III B. Similarly, in the case of the 4×4 cluster, the LESs are also $Sp(4)$ singlet at $\theta < 63^\circ$. This also suggests the spin-disordered GS with broken translational symmetry in the thermodynamic limit. Moreover, the gap between the GS and lowest singlet excited state is very small in a narrow regime (roughly $50^\circ \sim 60^\circ$), which implies that an intermediate phase may exist, exhibiting a different translational symmetry-breaking pattern from that with small values of θ. However, unlike the 1D case where we can justify the dimerization through finite-size scaling of the vanishing of the $Sp(4)$ singlet-singlet gap, it is impossible in two dimensions to detect the presence of the dimer states or plaquette states from the ED results. Thus we will resort to other approaches to investigate the GS profile in the following sections.

To further clarify, in Fig. 11 we present the spectra of LESs at each crystal momentum of $\Gamma = (0,0)$, $X = (\pi,0)$, and $M = (\pi,\pi)$, respectively. At $\theta \leqslant 63^\circ$, the states at the X point are lower than those at the M point, which are $Sp(4)$ singlets with the Casimir $C = 0$. These lowest singlet excitations along $(\pi,0)$ or $(0,\pi)$ would allow the GS to shift a lattice constant along the x or y direction, if the gap between these singlets vanishes in the thermodynamic limit. It would imply a fourfold degeneracy in the thermodynamic limit, breaking translational symmetry.

In comparison, as $\theta \geqslant 72^\circ$, the energy of states at the M point are lower than those at the X point, which are spin multiplet with 10-fold degeneracy and the $Sp(4)$ Casimir $C = 6$. Actually, these states are not the LESs which are five-fold degenerate located at the Γ point. Nevertheless, their energy splitting from the 10-fold states is very small, as shown in Fig. 10. In the thermodynamic limit, inspired by the QMC result of the occurrence of the long-range ordering in the $SU_B(4)$ case, we infer the long-range staggered Néel ordering of the $Sp(4)$ spin operators L_{ab} and a long-range uniform ordering of $Sp(4)$ vector operators n_a. Thus we infer a phase transition from spin-disordered GS to the Néel-like state-breaking $Sp(4)$ symmetry.

Let us make an analogy with the 2D spin-1/2 J_1-J_2 model.[56,57] In that case, the behavior of the low-lying energy levels indicates that the LESs with nonzero momentum are triplet while the system is a magnetic Néel ($J_2/J_1 \lesssim 0.4$) and collinear state ($J_2/J_1 \gtrsim 0.6$), corresponding to $\mathbf{K} = (\pi,\pi)$ and $(\pi,0)$, respectively. However, there exists an intermediate phase in $0.4 < J_2/J_1 < 0.6$, where the GS is a magnetic disordered state and the LES with nonzero momentum, $\vec{K} = (\pi,0)$, is singlet. In this region it has been conjectured that the GS is a dimerization state or a spin liquid (resonated-valence-bond state). Similarly, the low-lying energy behavior in our model implies that the GS is nonmagnetic at $\theta < 63^\circ$. On the other hand, at $\theta \geqslant 63^\circ$, the GS has spinful excitations and is relevant to the Néel state.

C. The magnetic structure form factor

In this subsection, we present the results of the magnetic structure form factors for the $N = 4 \times 4$ cluster. Two different

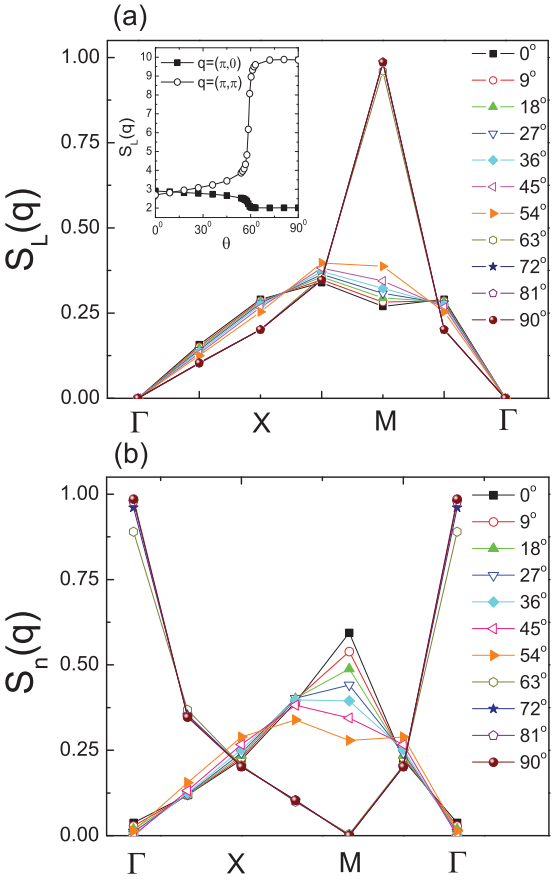

FIG. 12. (Color online) The magnetic structure factors for the 4×4 cluster. (a) The structure factors $S_L(\vec{q})$ for the $Sp(4)$ generator sector. The inset is the comparison between $S_L(\pi,0)$ and $S_L(\pi,\pi)$ versus θ. (b) The $Sp(4)$ vector structure factor $S_n(\vec{q})$.

structure form factors $S_L(\vec{q})$ and $S_n(\vec{q})$ are defined for the $Sp(4)$ generator and vector channels, respectively, as

$$S_L(\vec{q}) = \frac{1}{g_L N^2} \sum_{i,j,1\leqslant a<b\leqslant 5} e^{i\vec{q}\cdot(\vec{r}_i-\vec{r}_j)} \langle G|L_{ab}(i)L_{ab}(j)|G\rangle,$$
$$S_n(\vec{q}) = \frac{1}{g_n N^2} \sum_{i,j,a=1\sim 5} e^{i\vec{q}\cdot(\vec{r}_i-\vec{r}_j)} \langle G|n_a(i)n_a(j)|G\rangle, \quad (23)$$

where the normalization constants $g_L = 10$ and $g_n = 5$. $S_L(\vec{q})$ and $S_n(\vec{q})$ are the analogy of the Fourier transformation of $\langle G|\vec{S}_i \cdot \vec{S}_j|G\rangle$ in $SU(2)$ systems. If the long-range magnetic order appears, the magnetic structure factor converges to a finite value in the thermodynamic limit.[43,58]

The ED results of $S_L(\vec{q})$ for the 4×4 cluster are presented in Fig. 12(a). As $\theta \lesssim 60^\circ$, $S_L(\vec{q})$ distributes smoothly over all the momenta, and its maximum is located at $\vec{q} = (\pi, \frac{\pi}{2})$, which is slightly larger than other values of $\vec{q}$. In contrast, when $60^\circ \lesssim \theta \leqslant 90^\circ$, $S_L(\vec{q})$ peaks at $\vec{K}_M = (\pi,\pi)$. The $Sp(4)$ vector channel structure factor $S_n(\vec{q})$ is depicted in Fig. 12(b). At small values of θ, it peaks at the M point, exhibiting a dominate correlation at the momentum (π,π). As $\theta \gtrsim 60^\circ$, the peak changes to the Γ point and the M point becomes a minimum.

Along the $SU(4)_B$ line with $\theta = 90^\circ$, $S_n(\vec{q}) = S_L(\vec{q} + \vec{K}_M)$ due to the staggered definition of $Sp(4)$ vectors n_a in Eq. (12). This relation between $S_n(\vec{q})$ and $S_L(\vec{q} + \vec{K}_M)$ is consistent with the previous observation on the low-energy spectra in Fig. 10. As $\theta \geqslant 60^\circ$ there are two nearly degenerate excited states beyond the GS, having total momenta of (0,0) and (π,π). They correspond to the 5d vector representation with $C = 4$ and the 10d tensor representation with $C = 6$ in the $Sp(4)$ symmetry, respectively. The contributions to $S_n(\vec{K}_\Gamma)$ and $S_L(\vec{K}_M)$ mainly come from the matrix elements between the GS and the 5d vector states, and 10d antisymmetric tensor states, respectively. On the other hand, in the case of $SU(4)_A$ with $\theta = 45^\circ$, $S_n(\vec{q}) = S_L(\vec{q})$ for each $\vec{q}$.

These features highlight that the dominant Néel correlation of the $Sp(4)$ generator L_{ab}'s not only exhibits along the $SU(4)_B$ line but also extends to a finite regime with nonzero values of J_2. In the same parameter regime, the $Sp(4)$ vectors, n_a's, exhibit dominant uniform correlations. The critical value of θ of the onset of the outstanding $S_L(\pi,\pi)$ is in good agreement with the location of the level crossing shown in Fig. 10, implying a transition of the GS from a non-Néel state to a Néel type. The inset in Fig. 12(a) compares the $S_L(\vec{q})$ behavior at $\vec{q} = (\pi,0)$ and (π,π) versus θ. $S_L(\pi,0)$ changes little as varying θ. Therefore, it is inferred that only the Néel-type order exists at θ close to 90°. The magnetic ordering at $(\pi,0)$ should not appear in the 2D $Sp(4)$ system.

Next one may raise a natural question: What is the spin pattern for the Néel-order state as $\theta \to 90^\circ$? According to Eq. (12), its classic energy can be minimized by choosing a staggered configuration for $\langle G|L_{15}(i)|G\rangle = \langle G|L_{23}(i)|G\rangle = (-)^i \frac{1}{2}$ and a uniform configuration of $\langle G|n_4(i)|G\rangle = \pm\frac{1}{2}$. These correspond to the staggered arrangement in the 2D lattice by using the two components of $F_z = \pm\frac{3}{2}$, or by using the other two components of $F_z = \pm\frac{1}{2}$. These different classic Néel states can be connected by an $Sp(4)$ rotation.

D. The columnar dimer correlations

In this subsection, we discuss the possibility of the dimer-ordered state at intermediate values of θ. We define the susceptibility to a symmetry-breaking perturbation as

$$\chi(\delta) = -\frac{2[e(\delta) - e(0)]}{\delta^2}, \quad (24)$$

where $e(0)$ is the GS energy per site given by Hamiltonian Eq. (7) and $e(\delta)$ is Eq. (7) plus the corresponding perturbation term $-\delta\hat{O}$.[59,60] In the presence of long-range ordering, the corresponding susceptibility $\chi = \lim_{\delta\to 0}\chi(\delta)$ will diverge in the thermodynamic limit. It has been demonstrated that this approach can efficiently distinguish dimerized and non dimerized phases in the 1D J_1-J_2 spin-1/2 chain,[60] in which the phase boundary $J_2/J_1 \approx 0.24$ between these two phases.

Here we employ the same method to study the dimerization correlations. Although with small-size calculations, we are unable to determine the existence of long range order, it is still instructive to observe the feature of χ. We have used it to test the 1D $Sp(4)$ system with the perturbation term of $\hat{O} = \sum_i (-1)^i H_{ex}(i,i+1)$. At $\theta = 60^\circ$, we found the dramatic growing behavior of $\chi(\delta)$ upon decreasing δ and increasing the system size, which leads to a divergent χ in the thermodynamic limit. On the other hand, $\chi(\delta)$ at $\theta = 30^\circ$ has no tendency of divergence over decreasing δ.

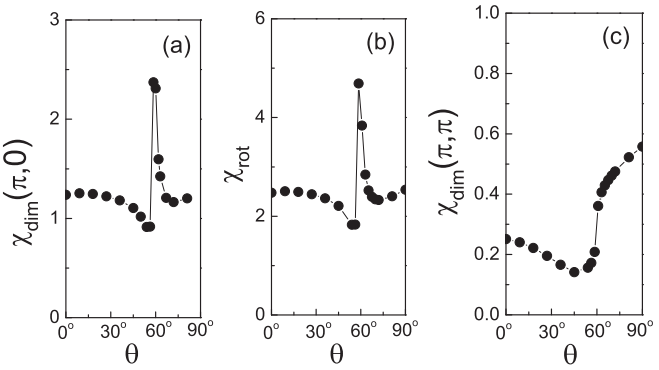

FIG. 13. The susceptibilities defined in Eq. (24) with respect to the perturbations O_{dim} and O_{rot} for the $N = 4 \times 4$ cluster. (a) $\chi_{dim}(\vec{Q})$ vs. θ at $\vec{Q} = (\pi,0)$; (b) χ_{rot} vs. θ; (c) $\chi_{dim}(\vec{Q})$ vs. θ at $\vec{Q} = (\pi,\pi)$. In both cases, a small value of $\delta = 0.01$ is taken to evaluate the susceptibilities. Both susceptibilities exhibit peaks around $\theta \approx 60^\circ \sim 70^\circ$.

This observation is consistent with our previous analytical and numerical studies: The 1D $Sp(4)$ system is either a gapless uniform liquid at $\theta \leqslant 45^\circ$ or a gapped dimerized state with the breaking of translation symmetry at $\theta > 45^\circ$.

Next we apply this method to the 2D system with the size of 4×4, and define two susceptibilities $\chi_{dim}(\vec{Q})$ and χ_{rot} for two perturbations of $\hat{O}_{dim}(\vec{Q})$ and $\hat{O}_{rot}$ as

$$\hat{O}_{dim}(\vec{Q}) = \sum_i \cos(\vec{Q} \cdot \vec{r}_i) H_{ex}(i, i+\hat{x}), \tag{25}$$

$$\hat{O}_{rot} = \sum_i [H_{ex}(i, i+\hat{x}) - H_{ex}(i, i+\hat{y})], \tag{26}$$

where $H_{ex}(i,j)$ is defined as one bond of Hamiltonian Eq. (7) without summation over i and j. Let us set $\vec{Q} = (\pi,0)$, thus $\chi_{dim}(\pi,0)$ corresponds to the instability to the columnar dimer configuration. Equations (25) and (26) break the translational symmetry along the x direction and rotational symmetry, respectively. The plaquette ordering maintains the four-fold rotational symmetry; thus it will lead to the divergence of $\chi_{dim}(\pi,0)$ but not χ_{rot}. The ED results for the susceptibilities with respect to the two perturbations vs. θ are shown in Fig. 13(a) and 13(b), respectively. A small value of $\delta = 0.01$ is taken. Both susceptibilities exhibit a peak at θ from 60° to 70°, which implies a tendency to breaking both translational and rotational symmetries. This shows that the columnar dimerization instead of the plaquette ordering is a promising instability in this regime in the thermodynamic limit. We have also calculated the susceptibility of $\chi_{dim}(\vec{Q})$ for $\vec{Q} = (\pi,\pi)$ which corresponds to the instability to the staggered dimer configuration in Fig. 13(c). Although the magnitudes of $\chi_{dim}(\pi,\pi)$ are smaller than $\chi_{dim}(\pi,0)$ and χ_{rot}, it suddenly raises up around $\theta = 60^\circ$.

E. The plaquette form factor

In this subsection, we consider the plaquette-type correlation. The GSs of the 4×4 cluster at $\theta \lesssim 60^\circ$ signal a different class from that in $\theta \geqslant 63^\circ$ in which the LESs are spin multiplet with $\vec{K} = (\pi,\pi)$. Here, the LESs remain $Sp(4)$ singlets with $\vec{K} = (\pi,0)$ or $(0,\pi)$. To further elucidate the GS profile, we

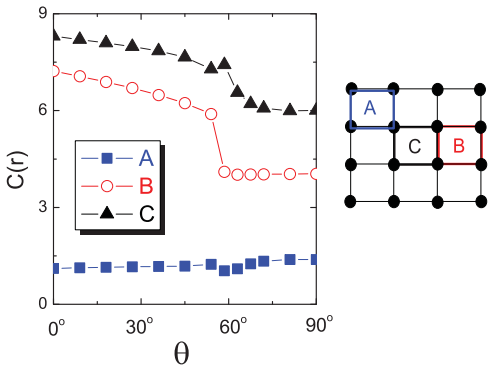

FIG. 14. (Color online) $C(\vec{r})$ defined in Eq. (27) versus θ. The positions of plaquette A, B, and C are defined on the right schematics. A (blue) is located at the corner whereas C (black) in the most middle one.

define the local Casimir for the plaquette centered at $\vec{r}$,

$$C(\vec{r}) = \langle G | \sum_{1 \leqslant a < b \leqslant 5} \left\{ \sum_i L_{ab}(i) \right\}^2 | G \rangle, \tag{27}$$

where i runs over the four sites of this plaquette. The $SU(2)$ version of Eq. (27) has been used to classify competing dimer and plaquette orders.[61] If the GS exhibits a strong plaquette pattern, for instance, indicated as phase **A** in Fig. 8, the magnitudes of $C(\vec{r})$ will have obvious spatial variations between NN plaquette. This is analogous to the 1D dimerization picture in Fig. 5(a), where the NN spin-spin correlations alternately exhibit strong and weak magnitudes. When the spins around a plaquette are strongly bound to form an $SU(4)$ singlet, $C(\vec{r})$ should be close to zero.

Figure 14 depicts the behavior of $C(\vec{r})$ at various values of θ for the 4×4 cluster. To explicitly reflect the plaquette formation, we use OBCs rather than periodic boundary conditions. In this case only C_{4v} point group symmetry is applicable in the ED. The $C(\vec{r})$ for the corner plaquette A is much smaller than 1/5 of those at the center C and the middle of the edge B for small values of θ. This is in sharp contrast to the 2D spin-1/2 model which renders $C(A) = 0.545$, $C(B) = 1.015$, and $C(C) = 1.282$, which only show the difference of the order of 1. The comparison suggests the pinning-down plaquette state in the 2D $Sp(4)$ system under the open boundary. We observe that $C(A)$ and $C(B)$ decrease while θ goes beyond 60°. It accounts for the formation of the plaquette-type pattern that weakens or even vanishes.

Combining the above observations, it is likely that for $\theta < 60^\circ$ the GS has a strong plaquette-like correlation that could be the resonate plaquette state proposed by Bossche *et al.*[40] or a certain spin liquid. It does survive not only along the $SU(4)_A$ line but also in a finite regime. Nevertheless, we have to emphasize that this picture cannot be conclusively determined due to finite-size effects and further larger-size calculations are needed to confirm.

V. CONCLUSION

In conclusion, we study an $Sp(4)/SO(5)$ spin Heisenberg model which can be realized by large-spin ultracold fermions

with $F = 3/2$. The $Sp(4)$ Heisenberg model describing the magnetic exchange at the insulating state of quarter-filling is simulated by ED and DMRG. In one dimention, our numerical results are in agreement with previous analytic studies. There are two competing phases: a gapped dimer phase with spin gap at $\theta > 45^\circ$ and a gapless spin liquid at $\theta \leqslant 45^\circ$. The phase boundary is identified as $\theta = 45^\circ$ which belongs to $SU(4)_A$-type symmetry. In the gapless spin liquid phase, the static correlation functions decay algebraically with four-site periodicity oscillations.

We also investigate the $Sp(4)$ spin model on a 2D square lattice up to 16 sites by means of the ED methods. Our numerical results show three competing correlations: Néel type, plaquette formation and columnar spin-Peierls dimerization, depending on θ's. Such observation can have phase behavior analogy in comparison with the speculated phase diagram depicted in Fig. 8. Due to the finite-size effects, however, we are unable to conclusively identify the existence of these phases and the phase boundaries based on the small cluster. More numerical studies are necessary to further explore the phase diagram in the thermodynamic limit.

ACKNOWLEDGMENTS

H. H. H. is grateful to helpful discussions with Stephan Rachel and computational facilities from Tunghai University. H. H. H. also appreciates Zi Cai and Cheng-Chien Chen for fruitful discussions and suggestions on exact diagonalization techniques. H. H. H. and C. W. are supported by NSF under No. DMR-1105945. Y. P. W. is supported by NSFC and 973-Project of MOST, China.

APPENDIX A: REPRESENTATION THEORY OF THE SIMPLE LIE GROUPS AND ALGEBRAS

The representation theory of Lie groups and algebra can be found in standard group theory textbooks.[62] Here we give a brief pedagogical introduction. Among the group generators, we choose the maximal set of generators that commute with each other as the *Cartan subalgebra* $\{H_i,(i = 1,\ldots,k)\}$, where k is called the rank of the Lie algebra. For example, the $SU(2)$ algebra is rank one, whose Cartan subalgebra contains only S_z. All other generators can be organized as eigenoperators of each generator in the Cartan sub-algebra, which are called *roots*. Roots always appear in terms of Hermitian conjugate pairs as $E_{j\pm}$ with the relation $E_{j-} = E_{j+}^\dagger$. They satisfy the commutation relations of

$$[H_i, E_{\pm j}] = \alpha_{\pm j}(i) E_{\pm j}, \tag{A1}$$

with $\vec{\alpha}_j = -\vec{\alpha}_{-j}$, where the ith elements of the vectors $\vec{\alpha}_{\pm j}$ are the eigenvalue of $E_{\pm j}$ with respect to H_i. For example, for the simplest $SU(2)$ case, the roots are $S_\pm = S_x \pm iS_y$ and $[Sz, S_\pm] = \pm S_\pm$, where $\alpha_\pm$ only have one component with $\alpha_\pm = \pm 1$.

Among all the roots, we fix the convention to use E_{+j} for *positive roots*, which means the first nonzero components of their $\vec{\alpha}_{+j}$ are positive. Positive roots can be decomposed into the linear combinations of *simple roots* with nonnegative integer coefficients. The number of simple roots of a simple Lie algebra equals to its rank. The *Cartan matrix* A of a simple Lie algebra is defined as

$$A_{ij} = 2\frac{(\vec{\alpha}_i, \vec{\alpha}_j)}{(\vec{\alpha}_i, \vec{\alpha}_i)}, \quad (i, j = 1,\ldots,k), \tag{A2}$$

where $\vec{\alpha}_i$ is the vector of eigenvalues of the simple root E_i; the inner products of α vectors are defined as

$$(\vec{\alpha}_i, \vec{\alpha}_j) = \sum_{l=1}^{k} \alpha_i(l)\alpha_j(l). \tag{A3}$$

The dimension of the Cartan matrix is the same as the Cartan subalgebra. For the $SU(2)$ group, the only positive and simple root is S_+, and the 1×1 Cartan matrix $A = 2$.

An important concept of the representations of the simple Lie algebra is *weight*. For a rank-k simple Lie algebra, its fundamental weights can be solved through its $k \times k$ Cartan matrix,

$$\vec{M}_i = \sum_j \vec{\alpha}_j (A^{-1})_{ji}, \quad (i = 1,\ldots,k). \tag{A4}$$

Any irreducible representation of a simple Lie algebra is uniquely determined by its highest weight $\vec{M}^*$, which can be written as a linear combination of the fundamental weights $\vec{M}_i$,

$$\vec{M}^* = \sum_i \mu_i \vec{M}_i, \quad (i = 1,\ldots,k), \tag{A5}$$

where μ's are nonnegative integers. The dimension of the representation M^* is

$$d(M^*) = \prod_{\text{positive roots}} \left[1 + \frac{(\vec{M}^*, \vec{\alpha}_i)}{(\vec{R}, \vec{\alpha}_i)}\right], \tag{A6}$$

with

$$\vec{R} = \frac{1}{2} \sum_{\text{positive roots}} \vec{\alpha}_i. \tag{A7}$$

Please notice that the product in Eq. (A6) and summation in Eq. (A7) take over all the positive roots. The value of the *Casimir* operator for the representation denoted by M^* is

$$C(\vec{M}^*) = (\vec{M}^*, \vec{M}^* + 2\vec{R}). \tag{A8}$$

For the simplest example of $SU(2)$, the only fundamental weight $M = 1/2$. The highest weights is just $M^* = S$, where S takes half-integer and integer numbers. Obviously, $d(S) = 2S + 1$ and $C(S) = S(S + 1)$, as expected.

APPENDIX B: THE $Sp(4)(SO(5))$ ALGEBRA

For convenience, we use the following symbols to represent the $Sp(4)(SO(5))$ generators $L_{ab}(1 \leqslant a < b \leqslant 5)$ defined in Eq. (5) as

$$L_{ab} = \begin{pmatrix} 0 & \mathrm{Re}\pi_x & \mathrm{Re}\pi_y & \mathrm{Re}\pi_z & Q \\ & 0 & -S_z & S_y & \mathrm{Im}\pi_x \\ & & 0 & -S_x & \mathrm{Im}\pi_y \\ & & & 0 & \mathrm{Im}\pi_z \\ & & & & 0 \end{pmatrix}, \tag{B1}$$

TABLE I. Cartan subalgebra and its roots. $[E_1,E_{-1}]=\frac{1}{6}(Q-S_z)$, $[E_2,E_{-2}]=\frac{1}{6}S_z$, $[E_3,E_{-3}]=\frac{1}{6}(Q+S_z)$, $[E_4,E_{-4}]=\frac{1}{6}Q$.

(Q,S_z)	Roots
$\alpha_{\pm1}=\pm(1,-1)$	$E_1=\frac{1}{\sqrt{24}}(\pi_x^\dagger-i\pi_y^\dagger);E_{-1}=\frac{1}{\sqrt{24}}(\pi_x+i\pi_y)$
$\alpha_{\pm2}=\pm(0,1)$	$E_2=\frac{1}{\sqrt{12}}(S_x+iS_y);E_{-2}=\frac{1}{\sqrt{12}}(S_x-iS_y)$
$\alpha_{\pm3}=\pm(1,1)$	$E_3=\frac{1}{\sqrt{24}}(\pi_x^\dagger+i\pi_y^\dagger);E_{-3}=\frac{1}{\sqrt{24}}(\pi_x-i\pi_y)$
$\alpha_{\pm4}=\pm(1,0)$	$E_4=\frac{1}{\sqrt{12}}\pi_z^\dagger;E_{-4}=\frac{1}{\sqrt{12}}\pi_z$

where

$$\begin{aligned}
\pi_x^\dagger &= \mathrm{Re}\pi_\mathrm{x}+\mathrm{iIm}\pi_\mathrm{x}=\psi^\dagger_{\frac{3}{2}}\psi_{-\frac{3}{2}}+\psi^\dagger_{\frac{1}{2}}\psi_{-\frac{1}{2}},\\
\pi_x &= \mathrm{Re}\pi_\mathrm{x}-\mathrm{iIm}\pi_\mathrm{x}=\psi^\dagger_{\frac{-3}{2}}\psi_{\frac{3}{2}}+\psi^\dagger_{-\frac{1}{2}}\psi_{\frac{1}{2}},\\
\pi_y^\dagger &= \mathrm{Re}\pi_\mathrm{y}+\mathrm{iIm}\pi_\mathrm{y}=-\mathrm{i}\big(\psi^\dagger_{\frac{3}{2}}\psi_{-\frac{3}{2}}-\psi^\dagger_{\frac{1}{2}}\psi_{-\frac{1}{2}}\big),\\
\pi_y &= \mathrm{Re}\pi_\mathrm{y}-\mathrm{iIm}\pi_\mathrm{y}=\mathrm{i}\big(\psi^\dagger_{\frac{-3}{2}}\psi_{\frac{3}{2}}-\psi^\dagger_{-\frac{1}{2}}\psi_{\frac{1}{2}}\big),\\
\pi_z^\dagger &= \mathrm{Re}\pi_\mathrm{z}+\mathrm{iIm}\pi_\mathrm{z}=\psi^\dagger_{\frac{3}{2}}\psi_{-\frac{1}{2}}-\psi^\dagger_{\frac{1}{2}}\psi_{-\frac{3}{2}},\\
\pi_z &= \mathrm{Re}\pi_\mathrm{z}-\mathrm{iIm}\pi_\mathrm{z}=\psi^\dagger_{-\frac{1}{2}}\psi_{\frac{3}{2}}-\psi^\dagger_{-\frac{3}{2}}\psi_{\frac{1}{2}},\\
S_+ &= S_x+iS_y=\psi^\dagger_{\frac{3}{2}}\psi_{\frac{1}{2}}-\psi^\dagger_{-\frac{1}{2}}\psi_{-\frac{3}{2}},\\
S_- &= S_x-iS_y=\psi^\dagger_{\frac{1}{2}}\psi_{\frac{3}{2}}-\psi^\dagger_{-\frac{3}{2}}\psi_{-\frac{1}{2}},\\
S_z &= \tfrac{1}{2}\big(\psi^\dagger_{\frac{3}{2}}\psi_{\frac{3}{2}}-\psi^\dagger_{\frac{1}{2}}\psi_{\frac{1}{2}}+\psi^\dagger_{-\frac{1}{2}}\psi_{-\frac{1}{2}}-\psi^\dagger_{-\frac{3}{2}}\psi_{-\frac{3}{2}}\big),\\
Q &= \tfrac{1}{2}\big(\psi^\dagger_{\frac{3}{2}}\psi_{\frac{3}{2}}+\psi^\dagger_{\frac{1}{2}}\psi_{\frac{1}{2}}-\psi^\dagger_{-\frac{1}{2}}\psi_{-\frac{1}{2}}-\psi^\dagger_{-\frac{3}{2}}\psi_{-\frac{3}{2}}\big).
\end{aligned}\tag{B2}$$

The 10 operators of $Sp(4)$ satisfy the commutation relations

$$[L_{ab},L_{cd}]=-i(\delta_{bc}L_{ad}+\delta_{ad}L_{bc}-\delta_{ac}L_{bd}-\delta_{bd}L_{ac}),\tag{B3}$$

which is rank-2 Lie algebra. Its Cartan subalgebra contains only two commutable generators $H_i(i=1,2)$, which can be chosen as $(H_1=S_z,H_2=Q)$. We group the other 8 generators as their eigenoperators, *i.e.*, roots as represented $E_{\pm1},E_{\pm2},E_{\pm3},E_{\pm4}$, whose eigenvalue vectors $\vec{\alpha}_{\pm j}$ are presented in Table. I. The simple roots are E_1 with $\vec{\alpha}_1=(1,-1)$ and and E_2 with $\vec{\alpha}_2=(0,1)$. The other roots can be represented

TABLE II. Some irreducible representations of the $Sp(4)/SO(5)$ group: the highest weights, dimensions, and Casimirs.

	(μ_1,μ_2)	M^*	$d(M^*)$	$C(\vec{M}^*)$
1	(0,0)	(0,0)	1	0
2	(0,1)	$(\frac{1}{2},\frac{1}{2})$	4	$\frac{5}{2}$
3	(1,0)	(1,0)	5	4
4	(0,2)	(1,1)	10	6
5	(2,0)	(2,0)	14	10
6	(1,1)	$(\frac{3}{2},\frac{1}{2})$	16	$\frac{15}{2}$
7	(1,2)	(2,1)	35	12
8	(0,3)	$(\frac{3}{2},\frac{3}{2})$	20	$\frac{21}{2}$

TABLE III. Cartan subalgebra and its roots. $[F_1,F_{-1}]=\frac{1}{8}(Q-S_z)$,$[F_2,F_{-2}]=\frac{1}{8}(S_z-n_4)$,$[F_3,F_{-3}]=\frac{1}{8}(S_z+n_4)$,$[F_4,F_{-4}]=\frac{1}{8}(Q+S_z)$,$[F_5,F_{-5}]=\frac{1}{8}(Q+n_4)$,$[F_6,F_{-6}]=\frac{1}{8}(Q-n_4)$.

(Q,S_z,n_4)	Roots
$\alpha_{\pm1}=\pm(1,-1,0)$	$F_1=\frac{1}{\sqrt{32}}(\pi_x^\dagger-i\pi_y^\dagger)=\frac{1}{\sqrt{8}}\psi^\dagger_{\frac{1}{2}}\psi_{-\frac{1}{2}}$
$\alpha_{\pm2}=\pm(0,1,-1)$	$F_2=\frac{(S_x+iS_y)-(n_2+in_3)}{\sqrt{32}}=\frac{1}{\sqrt{8}}\psi^\dagger_{-\frac{1}{2}}\psi_{-\frac{3}{2}}$
$\alpha_{\pm3}=\pm(0,1,1)$	$F_3=\frac{1}{\sqrt{32}}(S_x+iS_y+n_2+in_3)=\frac{1}{\sqrt{8}}\psi^\dagger_{\frac{3}{2}}\psi_{\frac{1}{2}}$
$\alpha_{\pm4}=\pm(1,1,0)$	$F_4=\frac{1}{\sqrt{32}}(\pi_x^\dagger+i\pi_y^\dagger)=\frac{1}{\sqrt{8}}\psi^\dagger_{\frac{3}{2}}\psi_{-\frac{3}{2}}$
$\alpha_{\pm5}=\pm(1,0,1)$	$F_5=\frac{1}{\sqrt{32}}(\pi_z^\dagger-i(n_1-in_5))=\frac{1}{\sqrt{8}}\psi^\dagger_{\frac{3}{2}}\psi_{-\frac{1}{2}}$
$\alpha_{\pm6}=\pm(1,0,-1)$	$F_6=\frac{1}{\sqrt{32}}(\pi_z^\dagger+i(n_1-in_5))=\frac{-1}{\sqrt{8}}\psi^\dagger_{\frac{1}{2}}\psi_{-\frac{3}{2}}$

as $E_3=E_1+2E_2,E_4=E_1+E_2$. The $Sp(4)/SO(5)$ Cartan matrix reads

$$A=\begin{pmatrix}2&-1\\-2&2\end{pmatrix}.\tag{B4}$$

We solve the fundamental weights as $\vec{M}_1=(1,0),\vec{M}_2=(\frac{1}{2},\frac{1}{2})$ from Eq. (A4). The highest weight $\vec{M}^*$ can be written as

$$\vec{M}^*=(m_1,m_2)=\left(\mu_1+\frac{\mu_2}{2},\frac{\mu_2}{2}\right),\tag{B5}$$

where $\mu_{1,2}$ are non-negative integers. The dimension of the corresponding representation is

$$d(\mu_1,\mu_2)=(1+\mu_1)(1+\mu_2)\left(1+\frac{2\mu_1+\mu_2}{3}\right)\times\left(1+\frac{\mu_1+\mu_2}{2}\right).\tag{B6}$$

The representation (μ_1,μ_2) belongs to the category of tensor or spinor representations of $Sp(4)$ when μ_2 is even or odd, respectively. The Casimir operator reads

$$\begin{aligned}C(\vec{M}^*)&=\sum_{a<b}L_{ab}^2=Q^2+S_z^2+6\sum_\alpha\{E_\alpha,E_{-\alpha}\}\\&=m_1(m_1+3)+m_2(m_2+1).\end{aligned}\tag{B7}$$

We summarize some frequently used representations of $Sp(4)(SO(5))$ in Table II. The representations with indices

TABLE IV. Some frequently used irreducible representations of the $SO(6)$ or $SU(4)$ group: the highest weight, dimension, and Casimir.

Rep	(μ_1,μ_2,μ_3)	$M^*(m_1,m_2,m_3)$	$d(M^*)$	Casimir
1	(0,0,0)	(0,0,0)	1	0
2	(0,0,1)	$(\frac{1}{2},\frac{1}{2},\frac{1}{2})$	4	$\frac{15}{4}$
3	(0,1,0)	$(\frac{1}{2},\frac{1}{2},\frac{-1}{2})$	4	$\frac{15}{4}$
4	(1,0,0)	(1,0,0)	6	5
5	(0,0,2)	(1,1,1)	10	9
6	(0,2,0)	(1,1,−1)	10	9
7	(0,1,1)	(1,1,0)	15	8
8	(2,0,0)	(2,0,0)	20	12

1 to 5 are particularly useful. They are the identity (1d), the fundamental spinor (4d), vector (5d), adjoint (10d), symmetric traceless tensor (14d) representations of the $SO(5)$ group, respectively.

APPENDIX C: $SU(4)(SO(6))$ ALGEBRA

The $SU(4)$ group is isomorphic to $SO(6)$. Their relation is similar to that between $SU(2)$ and $SO(3)$, or $Sp(4)$ and $SO(5)$. As represented in Eq. (5), L_{ab} and the five spin-quadrapole operators $n_a = \psi^\dagger_\alpha \Gamma^a_{\alpha\beta}\psi_\beta$ together form the 15 generators of the $SU(4)$ group. Explicitly, the generators of n_as are written as

$$\begin{aligned}
n_1 &= \frac{i}{2}\left(\psi^\dagger_{\frac{3}{2}}\psi_{-\frac{1}{2}} + \psi^\dagger_{\frac{1}{2}}\psi_{-\frac{3}{2}} - \psi^\dagger_{-\frac{1}{2}}\psi_{\frac{3}{2}} - \psi^\dagger_{-\frac{3}{2}}\psi_{\frac{1}{2}}\right),\\
n_2 &= \frac{1}{2}\left(\psi^\dagger_{\frac{3}{2}}\psi_{\frac{1}{2}} + \psi^\dagger_{\frac{1}{2}}\psi_{\frac{3}{2}} - \psi^\dagger_{-\frac{1}{2}}\psi_{-\frac{3}{2}} - \psi^\dagger_{-\frac{3}{2}}\psi_{-\frac{1}{2}}\right)\\
n_3 &= -\frac{i}{2}\left(\psi^\dagger_{\frac{3}{2}}\psi_{\frac{1}{2}} - \psi^\dagger_{\frac{1}{2}}\psi_{\frac{3}{2}} - \psi^\dagger_{-\frac{1}{2}}\psi_{-\frac{3}{2}} + \psi^\dagger_{-\frac{3}{2}}\psi_{-\frac{1}{2}}\right) \quad \text{(C1)}\\
n_4 &= \frac{1}{2}\left(\psi^\dagger_{\frac{3}{2}}\psi_{\frac{3}{2}} - \psi^\dagger_{\frac{1}{2}}\psi_{\frac{1}{2}} - \psi^\dagger_{-\frac{1}{2}}\psi_{-\frac{1}{2}} + \psi^\dagger_{-\frac{3}{2}}\psi_{-\frac{3}{2}}\right)\\
n_5 &= -\frac{1}{2}\left(\psi^\dagger_{\frac{3}{2}}\psi_{-\frac{1}{2}} + \psi^\dagger_{\frac{1}{2}}\psi_{-\frac{3}{2}} + \psi^\dagger_{-\frac{1}{2}}\psi_{\frac{3}{2}} + \psi^\dagger_{-\frac{3}{2}}\psi_{\frac{1}{2}}\right).
\end{aligned}$$

The rank of the $SU(4)$ group is three. We choose (Q, S_z, n_4) as the Cartan subalgebra and group the other 12 generators as roots as shown in Table III.

The simple roots are F_1, F_2, and F_3 with the eigenvalue vectors $\vec{\alpha}_1 = (1,-1,0)$, $\vec{\alpha}_2 = (0,1,-1)$, $\vec{\alpha}_3 = (0,1,1)$, respectively. The other positive roots are represented as $F_4 = F_1 + F_2 + F_3, F_5 = F_1 + F_3$ and $F_6 = F_1 + F_2$. The $SU(4)/SO(6)$ Cartan matrix reads

$$A = \begin{pmatrix} 2 & -1 & -1 \\ -1 & 2 & 0 \\ -1 & 0 & 2 \end{pmatrix}. \quad \text{(C2)}$$

The fundamental weights can be solved by using Eq. (A4)as

$$\vec{M}_1 = (1,0,0), \quad \vec{M}_2 = \left(\tfrac{1}{2},\tfrac{1}{2},-\tfrac{1}{2}\right), \quad \vec{M}_3 = \left(\tfrac{1}{2},\tfrac{1}{2},\tfrac{1}{2}\right). \quad \text{(C3)}$$

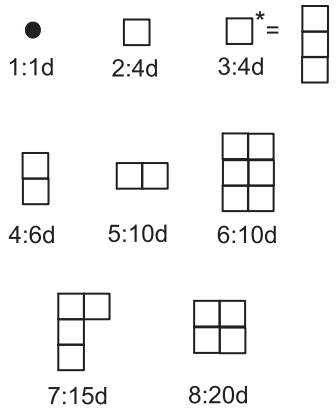

FIG. 15. The Young patterns of the $SU(4)$ representations 1 to 8 presented in Table IV.

The highest weight $\vec{M}^*$ of each representation can be chosen as

$$\begin{aligned}
\vec{M}^* &= (m_1,m_2,m_3) = \mu_1\vec{M}_1 + \mu_2\vec{M}_2 + \mu_3\vec{M}_3\\
&= \left(\mu_1 + \frac{\mu_2}{2} + \frac{\mu_3}{2}, \frac{\mu_2}{2} + \frac{\mu_3}{2}, -\frac{\mu_2}{2} + \frac{\mu_3}{2}\right). \quad \text{(C4)}
\end{aligned}$$

The dimension and Casimir of the representation $\vec{M}^*$ are represented as

$$\begin{aligned}
d(\vec{M}^*) &= (1+\mu_1)(1+\mu_1)(1+\mu_1)\left(1+\frac{\mu_1+\mu_2}{2}\right)\\
&\quad\times\left(1+\frac{\mu_1+\mu_3}{2}\right)\left(1+\frac{\mu_1+\mu_2+\mu_3}{3}\right), \quad \text{(C5)}\\
C(\vec{M}^*) &= H_1^2 + H_2^2 + H_3^2 + 8\sum_{\Delta^+}\{F_\alpha, F_{-\alpha}\}\\
&= m_1(m_1+4) + m_2(m_2+2) + m_3^2. \quad \text{(C6)}
\end{aligned}$$

We summarize some frequently used representations of $SU(4)(SO(6))$ in Table IV. Representations with indices from 1 to 6 are the identity (1d), the fundamental spinor (4d) and its complex conjugate (4d), the rank-2 antisymmetric tensor (6d), the rank-2 symmetric tensor (10d) and its complex conjugate (10d), and the adjoint (15d) representations, respectively. On the other hand, the Young pattern is often convenient for the representations of the $SU(N)$ group. The Young patterns of the representations from 1 to 8 in Table IV are shown in Fig. 15.

[1] B. J. DeSalvo, M. Yan, P. G. Mickelson, Y. N. Martinez de Escobar, and T. C. Killian, Phys. Rev. Lett. **105**, 030402 (2010).

[2] S. Taie, Y. Takasu, S. Sugawa, R. Yamazaki, T. Tsujimoto, R. Murakami, and Y. Takahashi, Phys. Rev. Lett. **105**, 190401 (2010).

[3] C. Wu, Physics **3**, 92 (2010).

[4] C. Wu, Mod. Phys. Lett. B **20**, 1707 (2006).

[5] S. K. Yip and T. L. Ho, Phys. Rev. A **59**, 4653 (1999).

[6] T. L. Ho and S. Yip, Phys. Rev. Lett. **82**, 247 (1999).

[7] S. Chen, C. Wu, S.-C. Zhang, and Y. Wang, Phys. Rev. B **72**, 214428 (2005).

[8] C. Xu and C. Wu, Phys. Rev. B **77**, 134449 (2008).

[9] C. Wu, K. Sun, E. Fradkin, and S. C. Zhang, Phys. Rev. B **75**, 115103 (2007).

[10] C. Wu, J. P. Hu, and S. C. Zhang, Phys. Rev. Lett. **91**, 186402 (2003).

[11] C. Wu, Phys. Rev. Lett. **95**, 266404 (2005).

[12] C. Wu, J. Hu, and S. Zhang, Int. J. Mod. Phys. B **24**, 311 (2010).

[13] S. Capponi, G. Roux, P. Azaria, E. Boulat, and P. Lecheminant, Phys. Rev. B **75**, 100503(R) (2007).

[14] H.-H. Tu, G.-M. Zhang, and L. Yu, Phys. Rev. B **74**, 174404 (2006).

[15] H.-H. Tu, G.-M. Zhang, and L. Yu, Phys. Rev. B **76**, 014438 (2007).

[16] D. Zheng, G.-M. Zhang, T. Xiang, and D.-H. Lee, Phys. Rev. B **83**, 014409 (2011).

[17]J. Zang, H.-C. Jiang, Z.-Y. Weng, and S.-C. Zhang, Phys. Rev. B **81**, 224430 (2010).
[18]D. H. Lee, G.-M. Zhang, T. Xiang, Nucl. Phys. B **846**, 607 (2011).
[19]E. Szirmai and M. Lewenstein, Europhys. Lett. **93**, 66005 (2011).
[20]D. Controzzi and A. M. Tsvelik, Phys. Rev. Lett. **96**, 97205 (2006).
[21]Y. Jiang, J. Cao, and Y. Wang, e-print arXiv:1006.2118 (2010).
[22]K. Hattori, J. Phys. Soc. Jpn. **74**, 3135 (2005).
[23]P. Lecheminant, E. Boulat, and P. Azaria, Phys. Rev. Lett. **95**, 240402 (2005).
[24]P. Lecheminant, P. Azaria, and E. Boulat, Nucl. Phys. B **798**, 443 (2008).
[25]D. Lee, Phys. Rev. Lett. **98**, 182501 (2007).
[26]A. V. Gorshkov, M. Hermele, V. Gurarie, C. Xu, P. S. Julienne, J. Ye, P. Zoller, E. Demler, M. D. Lukin, and A. M. Rey, Nat. Phys. **6**, 289 (2010).
[27]M. Hermele, V. Gurarie, and A. M. Rey, Phys. Rev. Lett. **103**, 135301 (2009).
[28]C. Xu, Phys. Rev. B **81**, 144431 (2010).
[29]M. A. Cazalilla, A. F. Ho, and M. Ueda, New J. Phys. **11**, 103033 (2009).
[30]R. Flint, M. Dzero, and P. Coleman, Nat. Phys. **4**, 643 (2008).
[31]R. Flint and P. Coleman, Phys. Rev. B **79**, 014424 (2009).
[32]S. Rachel, R. Thomale, M. Führinger, P. Schmitteckert, and M. Greiter, Phys. Rev. B **80**, 180420(R) (2009).
[33]H. Nonne, P. Lecheminant, S. Capponi, G. Roux, and E. Boulat, Phys. Rev. B **81**, 020408(R) (2010).
[34]A. K. Kolezhuk and T. Vekua, Phys. Rev. B **83**, 014418 (2011).
[35]S. R. White, Phys. Rev. Lett. **69**, 2863 (1992).
[36]S. R. White, Phys. Rev. B **48**, 10345 (1993).
[37]K. I. Kugel' and D. I. Khomskii, Usp. Fiz. Nauk **136**, 631 (1982).
[38]B. Sutherland, Phys. Rev. B **12**, 3795 (1975).
[39]Y. Q. Li, M. Ma, D. N. Shi, and F. C. Zhang, Phys. Rev. Lett. **81**, 3527 (1998).
[40]M. V. D. Bossche, F. C. Zhang, and F. Mila, Eur. Phys. J. B **17**, 367 (2000).
[41]M. van den Bossche, P. Azaria, P. Lecheminant, and F. Mila, Phys. Rev. Lett. **86**, 4124 (2001).
[42]A. Mishra, M. Ma, and F. C. Zhang, Phys. Rev. B **65**, 214411 (2002).
[43]K. Harada, N. Kawashima, and M. Troyer, Phys. Rev. Lett. **90**, 117203 (2003).
[44]N. Read and S. Sachdev, Phys. Rev. B **42**, 4568 (1990).
[45]E. H. Lieb, T. Schultz, and D. J. Mattis, Ann. Phys. (NY) **16**, 407 (1961).
[46]Y. Yamashita, N. Shibata, and K. Ueda, Phys. Rev. B **58**, 9114 (1998).
[47]P. Azaria, A. O. Gogolin, P. Lecheminant, and A. A. Nersesyan, Phys. Rev. Lett. **83**, 624 (1999).
[48]G. Fáth, O. Ligeza, and J. Sólyom, Phys. Rev. B **63**, 134403 (2001).
[49]H.-H. Hung, C.-D. Gong, Y.-C. Chen, and M.-F. Yang, Phys. Rev. B **73**, 224433 (2006).
[50]I. Affleck, Nucl. Phys. B **265**, 409 (1986).
[51]G. M. Zhang and S. Q. Shen, Phys. Rev. Lett. **87**, 157201 (2001).
[52]F. Wang and A. Vishwanath, Phys. Rev. B **80**, 064413 (2009).
[53]S. Rachel and M. Greiter, Phys. Rev. B **78**, 134415 (2008).
[54]Z. Cai, S. Chen, and Y. Wang, J. Phys.: Condens. Matter **21**, 456009 (2009).
[55]S. Pankov, R. Moessner, and S. L. Sondhi, Phys. Rev. B **76**, 104436 (2007).
[56]E. Dagotto and A. Moreo, Phys. Rev. B **39**, 4744 (1989).
[57]E. Dagotto and A. Moreo, Phys. Rev. Lett. **63**, 2148 (1989).
[58]H. J. Schulz and T. A. L. Ziman, Europhys. Lett. **18**, 355 (1992).
[59]G. Santoro, S. Sorella, L. Guidoni, A. Parola, and E. Tosatti, Phys. Rev. Lett. **83**, 3065 (1999).
[60]L. Capriotti and S. Sorella, Phys. Rev. Lett. **84**, 3173 (2000).
[61]J. Richter and N. B. Ivanove, Czech. J. Phys. **46**, 1919 (1996).
[62]Z. Ma, *Group Theory for Physicists* (World Scientific, Singapure, 2008).